A High Gain Inverse Concentric Yagi Director Antenna for 5G Millimeter-Wave and Satellite Communication

Raqeebur Rehman[1], Javaid A. Sheikh[1, *], Khurshed A. Shah[2], and Ghulam M. Bhat[1]

Abstract—A novel high gain two-port planar antenna for 5G millimeter-wave and satellite band is presented. The proposed antenna besides working in the millimeter-wave range has an added feature to work for the satellite X-band as well. The antenna has a miniaturized low-cost planar geometry having the dimensions of $1.83\lambda \times 1.83\lambda \times 0.07\lambda$ at 27.5 GHz, designed and fabricated on a Rogers RT/duroid substrate of thickness 0.8 mm. The proposed antenna has return loss values of 12.34 dB and 17.94 dB for the two resonant millimeter-wave frequencies of 27.24 GHz and 28.88 GHz respectively and 12.66 dB for the satellite band frequency of 8.42 GHz. The antenna attains a peak gain of 10.2 dBi for 28 GHz millimeter-wave band and 6.2 dBi for satellite X-band by exploiting an inverse microstrip Yagi director geometry. The isolation between two ports has been found satisfactory thus making it operate efficiently for the available Ka and X band capacity of the Wideband Global Satcom system (WGS). The experimental results regarding the fabricated prototype are presented and compared with the simulated results, which are in good agreement. The performance of the proposed antenna regarding radiation efficiency, directivity, gain, radiation pattern, and good isolation between the two ports makes the antenna employed as a suitable candidate for satellite communication and especially for 5G millimeter-wave communication.

1. INTRODUCTION

The millimeter-wave band turns out to be the most potential solution for fifth-generation mobile communication due to the accessibility of a wide spectrum [1, 2]. However, the signal attenuation and propagation loss of millimeter-waves in the atmosphere poses a serious challenge for the incorporation of 5G Networks. The solution will be to choose high gain antennas with better directivities and good radiation efficiencies to maintain the high speed and high-capacity communication link intact [3, 4]. The reduction in the size of antennas at very high millimeter-wave frequencies to the scale of a few millimeters poses another challenge for the deployment of the traditional antennas like Yagi, horns, sector antennas, and dipole arrays despite their good directivities and high gains at specified geometries [5–10]. Further, the cost regarding the implementation of such antennas at millimeter-wave band increases to a much higher level. So, the requirement is to incorporate low-cost, compact, miniaturized, and high gain antennas for 5G millimeter-wave links. The compactness and miniaturization can be achieved in the planar antennas for the facilitation of higher spectral efficiency, less interference, and better coverage of signal. The concept of inter-element spacing of half-wavelength and specific feeding techniques can be introduced for antenna arrays for the achievement of much higher gains and better directivity. But to maintain a high front-to-back ratio of antenna field patterns, the design of geometries regarding millimeter-wave antennas has to be chosen with keen care to circumvent the formation of high side lobes. Moreover, for millimeter-wave antennas, the emerging need will be for low complexity, low cost,

* Corresponding author: Javaid A. Sheikh (sheikhjavaid@uok.edu.in).
[1] Department of Electronics, University of Kashmir, Srinagar, India. [2] Department of Physics, S.P College, Cluster University, Srinagar, India.

compact size, wideband, high gain, easy implementation, and efficient integration ability with other circuitry. Higher gain, directivity, and bandwidth can be achieved utilizing Horn and Yagi antennas at millimeter-wave frequency bands, but their bulky shapes and huge sizes restrict them to easily integrate with planar microstrip circuitry. In addition, Ka-band mmWave frequencies such as 27.5–28.5 GHz or 37–40 GHz can be used in combination with X-band frequencies for the support of military satellite communication like Wideband Global Satcom system (WGS). The group of military communication satellites procured by the U.S. Air force known as WGS system provides combined capacity for both Ka and X-band frequencies. The X-band frequencies in the range 7.25 GHz to 7.75 GHz (Space to Earth) and 7.9 GHz to 8.4 GHz (Earth to Space) designated by the International Telecommunication Union (ITU) for satellite communication are used in the WGS system to make a compromise between various characteristics of higher mmWave frequency bands suited to military applications. The characteristics include signal attenuation due to the atmosphere, rain resilience, and coverage. X-band provides much better rain resilience and remote coverage than higher frequencies such as Ka or Ku (used for satellite communication as well) allowing a better and high link availability of almost 99%. Thus, in WGS satellite communication if uplink (Earth to Space) mmWave Ka frequency signals do not have a good coverage and signal attenuation due to rain fade is dominant, the problem can be managed by X-band uplink frequency as it is below all those frequencies which are severely attenuated by precipitation. Hence, there is a demand for the unique design of the antennas operating simultaneously for both mmWave and X-band frequencies with miniaturized sizes, low cost, high directivity, and low profile to be deployed for high gain antenna array configuration for WGS satellite communication. The antennas of this type may be used for both 5G mmWave mobile communication and WGS satellite communication. Some unique miniaturization techniques employed in some novel antennas have been reported recently, but most of them fail to achieve the high gain and directivity requirement of 5G mmWave and satellite communication. Apart from this, a very good contribution to 5G millimeter-wave antennas and Ku-band satellite antennas has been outlined in the literature. Fan et al. [11] have proposed a wideband conical-beam omnidirectional antenna with horizontal polarisation for millimeter-wave applications. There is 22.9% impedance bandwidth achievement in the resonant frequency band of 39–49.3 GHz with a better radiation pattern than the design presented in [24]. The gain in the designated band extends from 4.6 to 6 dBi. Due to the incorporation of SIW (Substrate Integrated Waveguide) radial power divider and a conical reflector, it transpires with minimum losses and proves as a good prototype for millimeter-wave communication. However, following comparison with the conventional millimeter-wave antennas having planar structures, the design turns a little bit convoluted. In [12], a planar and dual-band MIMO millimeter-wave antenna for 5G applications has been presented. The antenna comprises two monopole elements to achieve dual-band operation at 27 GHz and 39 GHz and is designed on Rogers 4003C dielectric. The antenna besides achieving a good radiation efficiency of 98–99% has a peak gain extending from 5 to 5.7 dBi with a mutual coupling of 25 to 30 dB between the ports and a very low envelope correlation coefficient of value 10^{-4}. The authors have succeeded to develop a low-profile antenna with good miniaturization and an acceptable gain, but the use of monopole elements has not resulted in a much directive radiation pattern. In [13], a multi-beam antenna array with tapered slots characteristic has been reported for massive MIMO mmWave communication. There is a low complexity related to the antenna geometry. With the unique incorporation of the SIW feeding technique, the integration ability of the given antenna with the planar circuits has been eased to a better extent. The antenna section elements have been spaced efficiently to fulfill the half-wavelength criteria. For each antenna element, the gain ranges from 8.2 to 9.6 dBi in the operating frequency of 24–32 GHz. A very good contribution has been provided to massive MIMO mmWave systems by the authors in this design. Other antennas are also presented having meta-material unit cells with wide-angle scan characteristics. These antennas are usually accompanied by a meta-material surface on which the specified geometries are printed consisting of radiating microstrip structures. The E-field of antennas is directed to propagate in specified directions with the employment of meta-material unit cells. Kumar et al. [14] have proposed a CPW-fed strip compact square loaded slot antenna with circular polarization for satellite communications in which a grounded L-strip, a grounded pair of spiral-shaped slots, and a slot in a rectangular shape in the lower left CPW ground plane are responsible for the gain of dual CP. A modified perturbation in the ground plane and CPW structure also leads to the improvement in dual CP. The antenna arrives at a gain value with a peak of 6.36 dBic, a dual-band characteristic, and

3 dB axial-ratio bandwidths in dual bands in the frequency band of 3–14 GHz. This antenna suits best for the wideband wireless and downlink Ku-band frequency but cannot be used for higher frequencies as a result of much higher losses due to coplanar profile. Though all the reported antennas [16–23] have some distinct and special characteristics, most of them specify a limit to attain the demanded radiation characteristics like radiation efficiency, good gain, and directivity. Moreover, these antenna designs fail to attain the required compactness, integration capability, low-cost characteristic, easy mounting, etc. Though their implementation and deployment turn out to be a little bit complicated chore, the authors have tried their best and attained a good milestone for providing a trade-off and a better solution for the limitations of 5G millimeter-wave communication.

Keeping the above constraints in view, a compact high gain two-port antenna for 5G millimeter-wave and WGS satellite communication is presented which is a low-cost planar structure consisting of an oblique slotted microstrip mini-patch responsible for mmWave radiation at 28 GHz band fed by a 0.6 mm feedline and surrounded by inverse concentric Yagi microstrip directors. The antenna has a simple planar geometry with a defected ground structure. Also, it is a highly miniaturized structure and besides resonating at the 28 GHz band also has an added feature to be employed in WGS X-band satellite communication as well. One port of the proposed antenna corresponds to 5G millimeter-wave frequency and the other one to X-band satellite frequency. The antenna achieves a good impedance bandwidth and a better gain than the reported antennas for both applications. The two ports of the proposed antenna can be used simultaneously or in a multiplexed manner for WGS satellite communication due to its good port isolation characteristic. Hence the antenna can serve as a sterling candidate for 5G millimeter-wave mobile communication and WGS satellite communication as it is highly compact, highly miniaturized with better gain, directivity, and radiation efficiency.

2. ANTENNA GEOMETRY, OPERATING MODE AND ANALYSIS

2.1. Antenna Layout

Figure 1 depicts the full geometrical design of the proposed antenna. The proposed antenna is designed on a 0.8 mm Rogers RT/duroid (5880) substrate having a dielectric value of 2.2 and a loss factor value of 0.0009. The defected ground structure (DGS) comprises a middle vertical rectangular strip integrated with two concentric microstrip rings and a vertical slot of a specific dimension near the mmWave port of the antenna to elongate the path of the surface current. The DGS is also accompanied by two vertical and identical rectangular strips towards the left and right. The ground plane of the proposed antenna has asymmetrical geometry from Port 1 and Port 2 side excluding the vertical rectangular slot on the middle strip. The substrate of the antenna is square-shaped and has a side dimension of 20 mm which is
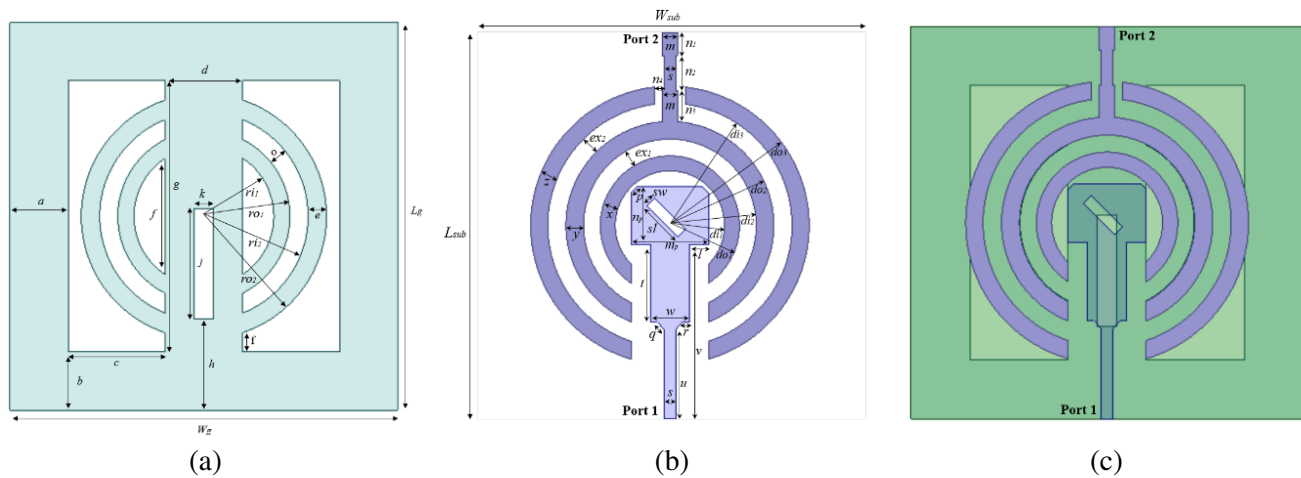
Figure 1. Layout of the proposed two-port antenna. (a) Bottom view. (b) Top view. (c) Complete view.

also the width of the defected ground. The top radiating structure of the antenna comprises an oblique slotted rectangular mini patch responsible for mmWave radiation fed by a 2 mm wide feed tapered with a 0.6 mm feedline. The rectangular mini-patch is surrounded by inverse concentric Yagi Uda microstrip directors for the enhancement of the peak gain of the proposed antenna in specified 5G mmWave band to 10.2 dBi and for specified X-band to 6.2 dBi. Similarly, the 2nd Yagi microstrip director is fed by a stepped impedance of width 0.8 mm from port 2 side to make the proposed antenna work as an X-band antenna. The proposed antenna can be viewed as a concentric circular Yagi director antenna for X-band and inverse concentric circular Yagi director antenna for 5G mmWave band. When the proposed antenna is utilized as an X-band antenna, the 2nd circular microstrip acts as the feed element, the outer microstrip as the reflector, and the inner microstrip surrounding the mmWave mini-patch as the director. When it is used as a 5G millimeter-wave antenna, the oblique slotted mini-patch acts as the main radiating element whose radiation is confined and concentrated by surrounding 1st, 2nd, and 3rd inverse concentric Yagi directors (can be treated as three concentric reflectors as well for this configuration and hence the name given is inverse). This arrangement can be understood as if the feed element is placed after the last director of a conventional Yagi Uda antenna, and in the proposed design, the directors are concentric. The millimeter-wave frequency is applied via 0.6 mm feed, and the satellite X-band frequency is applied via stepped impedance feed. For 5G mmWave mobile communication, only port 1 is excited; port 2 is not given any input; and the proposed antenna works as a 5G millimeter-wave antenna for mobile communication. For WGS satellite communication, both the ports can be excited simultaneously or in an alternate/multiplexed manner according to the need depending upon the weather conditions to make the proposed antenna work as an efficient uplink (Earth to Space) antenna for the WGS system. The full design process and the parametric study of the proposed antenna are carried out using Ansys HFSS V.15 simulator. The variables associated with the geometry and design of the antenna are elucidated below and listed in Table 1.

Table 1. Design variables of the proposed two-port antenna.

Parameter	Value (mm)	Parameter	Value (mm)	Parameter	Value (mm)
L_g	20	l	1	x	0.77
W_g	20	m	0.8	y	0.91
ri_1	3.6	f	1	z	0.88
ri_2	5.37	o	0.93	m_p	4
ro_1	4.44	n_1	1.2	n_p	3
ro_2	6.32	n_2	1.8	sl	2.26
a	3	n_3	1.62	sw	0.56
b	3	n_4	0.5	ex_1	0.86
c	5	p	0.42	ex_2	0.93
d	4	q	0.53	di_1	2.82
e	0.95	r	0.35	di_2	4.47
f	6	s	0.6	di_3	6.32
g	14	t	4	do_1	3.6
h	4.7	u	4.6	do_2	5.38
j	5.7	v	9	do_3	7.21
k	1	w	2	$L_{sub} = W_{sub}$	20

2.2. Operating Mode

There are two modes of operation for the proposed antenna in WGS applications: Simultaneous port mode and Multiplexed/Alternate port mode. In Simultaneous port mode, both the antenna ports are excited simultaneously with mmWave frequency at port 1 and X-band frequency at port 2. The

antenna works well for simultaneous port excitations as it has good port isolation of 15–25 dB. In Multiplexed/Alternate port mode, the antenna ports are excited with port 1 active and port 2 inactive, and in the next instant port 2 is active and port 1 inactive. This port selection procedure is provided to ensure the efficient transmission of the signal for uplink (Earth to Space) as the X-band signals enjoy a natural advantage and are not attenuated due to precipitation and rain fade providing a much better signal coverage and high throughput making it ideal for military applications in the toughest weather conditions. In contrast to this, the mmWave Ka-band signals easily get attenuated due to precipitation though this band provides much higher bandwidth and can handle a high amount of data stream.

Here L_g and W_g correspond to the length and width of the defected ground which is also equal to the substrate length and width, L_{sub} and W_{sub}, respectively. m_p and n_p denote the length and width of the mini-patch, and sl and sw represent the oblique slot dimensions on the mini-patch of the proposed geometry. Variables ri_1, ri_2 and ro_1, ro_2 represent the inner and outer radii of the concentric microstrip rings attached with the middle vertical strip on the ground plane of the proposed antenna, respectively. Similarly, parameters di_1, di_2, di_3 and do_1, do_2, do_3 denote the inner and outer radii of the concentric Yagi directors from the center of the presented antenna, respectively. Also, variables m, s, n_1, n_2, n_3, n_4 designate the dimensions of the stepped impedance attached with the second concentric director. The other parameters x, y, z and ex_1, ex_2 specify the sequential width of the microstrip Yagi directors and the separation between the directors observed from center to outwards of the proposed structure, respectively. Eventually, the remaining design variables are described in Fig. 1, and their corresponding numerical values are given in Table 1 along with already explained ones.

2.3. Analysis

The planar microstrip antenna analysis can be carried out by following several methods like the FDTD model, Method of moments, Transmission line model, and the Cavity model. These modeling methods are selective and widely employed methods for planar antenna analysis. Providing a better physical insight, the transmission line model is the easiest of other methods and has been utilized for the proposed two-port planar antenna as well. The proposed antenna along with the inverse concentric Yagi directors is designed by following Equations (1) to (8).

$$L = L_{eff} - 2\Delta L \tag{1}$$

Here, L denotes the actual length of the mini-patch.

$$L_{eff} = \frac{c_0}{2f_r\sqrt{\varepsilon_{reff}}} \tag{2}$$

L_{eff} denotes the effective length, f_r the resonant mmWave frequency, and C_0 the free space speed of light.

$$\text{and} \quad \Delta L = 0.412h\frac{(\varepsilon_{reff} + 0.3)\left(\frac{w}{h} + 0.264\right)}{(\varepsilon_{reff} - 0.258)\left(\frac{w}{h} + 0.8\right)} \tag{3}$$

ΔL denotes the increment in length as a result of fringing, w the width, and h the thickness of the substrate.

$$\text{Also,} \quad \varepsilon_{reff} = \frac{\varepsilon_r + 1}{2} + \frac{\varepsilon_r - 1}{2}\left[\frac{1}{\sqrt{1 + 12\frac{h}{w}}}\right] \tag{4}$$

ε_{reff} is the effective dielectric constant of the material, and ε_r is the actual dielectric constant.

Upon the substitution of Equations (2), (3), and (4) in Equation (1), the actual length of the mini-patch is given by

$$L = \frac{c_0}{2f_r\sqrt{\varepsilon_{reff}}} - 0.824h\frac{(\varepsilon_{reff} + 0.3)\left(\frac{w}{h} + 0.264\right)}{(\varepsilon_{reff} - 0.258)\left(\frac{w}{h} + 0.8\right)} \tag{5}$$

$$\text{Also,} \quad W = \frac{1}{2f_r\sqrt{\mu_0\varepsilon_0}}\sqrt{\frac{2}{\varepsilon_r+1}} = \frac{c_0}{2f_r}\sqrt{\frac{2}{\varepsilon_r+1}} \tag{6}$$

W denotes the width of mini-patch; f_r is the resonant mmWave frequency; μ_0 and ε_0 are the permeability and permittivity of free space.

Here, each of the Yagi directors can be treated as a circular loop, and the actual radius, rc, of one of the directors is given by

$$rc = \frac{F}{\left\{1 + \frac{2h}{\pi\varepsilon_r F}\left[\ln\left(\frac{\pi F}{2h}\right) + 1.7726\right]\right\}^{\frac{1}{2}}} \tag{7}$$

Here, h is the substrate height, ε_r the actual dielectric constant, and F the factor required to calculate the radius of the directors from the center of the mini-patch and is calculated below.

$$F = \frac{8.791 \times 10^9}{f_r\sqrt{\varepsilon_r}} = 0.216 \text{ (in our proposed design at } 27.5\,\text{GHz)}$$

In Equation (7), the fringing effect is not included which makes the geometry a bit electrically larger. Hence, the effective radius, rc_{eff}, for the director as a result of fringing may be calculated as,

$$rc_{eff} = rc\left\{1 + \frac{2h}{\pi\varepsilon_r a}\left[\ln\left(\frac{\pi rc}{2h}\right) + 1.7726\right]\right\}^{\frac{1}{2}} \tag{8}$$

where h is the thickness of the substrate, rc the actual radius of one of the directors, and ε_r the actual dielectric constant.

Using the equations discussed, the proposed antenna's mini-patch, the attached microstrip feed along with the concentric directors and stepped impedance have been designed carefully with optimized dimensions resulting in a better impedance match at the two ports and hence much better radiation efficiency.

3. DEVELOPMENTAL STAGES OF THE ANTENNA WITH PARAMETRIC ANALYSIS

A full-fledged parametric process has been carried to develop the proposed antenna as a novel and compact geometry with optimized dimensions. The full design process along with the parametric simulation results is carried out in Ansys EM tool, High-Frequency Structure Simulator (HFSS v.15). Fig. 2 depicts the design stages of the antenna along with the final proposed geometry.

Stage (A) forms the basic geometry of the antenna with two vertical slots of width 5 mm and length 14 mm each, forming a vertical microstrip of width 4 mm in the middle of the defected ground plane. The radiating structure for this stage includes a mini-patch of dimension $4 \times 3\,\text{mm}^2$ integrated with a microstrip section of width 2 mm followed by a tapered feed line of 0.6 mm width. This basic geometry of the antenna attains a return loss (RL) of 15.69 dB at a central frequency of 28.42 GHz with a peak gain of 9.21 dBi. This structure is a matched geometry with a VSWR value of 1.39. The simulated return loss and E-plane gain of this stage are shown in Figs. 3(a) and 3(b). The figures show that the basic geometry of the proposed antenna has a return loss value $\leq 10\,\text{dB}$ from 27.77 GHz to 29 GHz achieving an impedance bandwidth of 4.32% with a maximum simulated gain of 9.21 dBi in the E-plane. The 2nd stage (B) is formed by adding two concentric microstrip circular rings to the middle vertical strip of the defected ground of stage 1st (A). The RL in dB and E-plane gain of the stage (B) are depicted in Figs. 4(a) and 4(b). The 2nd stage shows a betterment in return loss attaining a value of 21.80 dB at 28.44 GHz with a reduction in peak gain to a value of 8.37 dBi. The 2nd stage (B) shows a better impedance match obtaining a VSWR value of 1.17. The impedance bandwidth for this stage is 4.14% at 28.44 GHz. Stage (C) is formed with the inclusion of a vertical slot of dimension $1 \times 5.7\,\text{mm}^2$ on the middle vertical strip of the ground plane of stage (B). The 3rd stage (C) further improves the return loss to 23.72 dB at 28.62 GHz with a better impedance match obtaining a VSWR value of 1.13. The impedance bandwidth is 4.26% at 28.62 GHz with RL $\leq 10\,\text{dB}$ from 27.97 GHz to 29.19 GHz. This
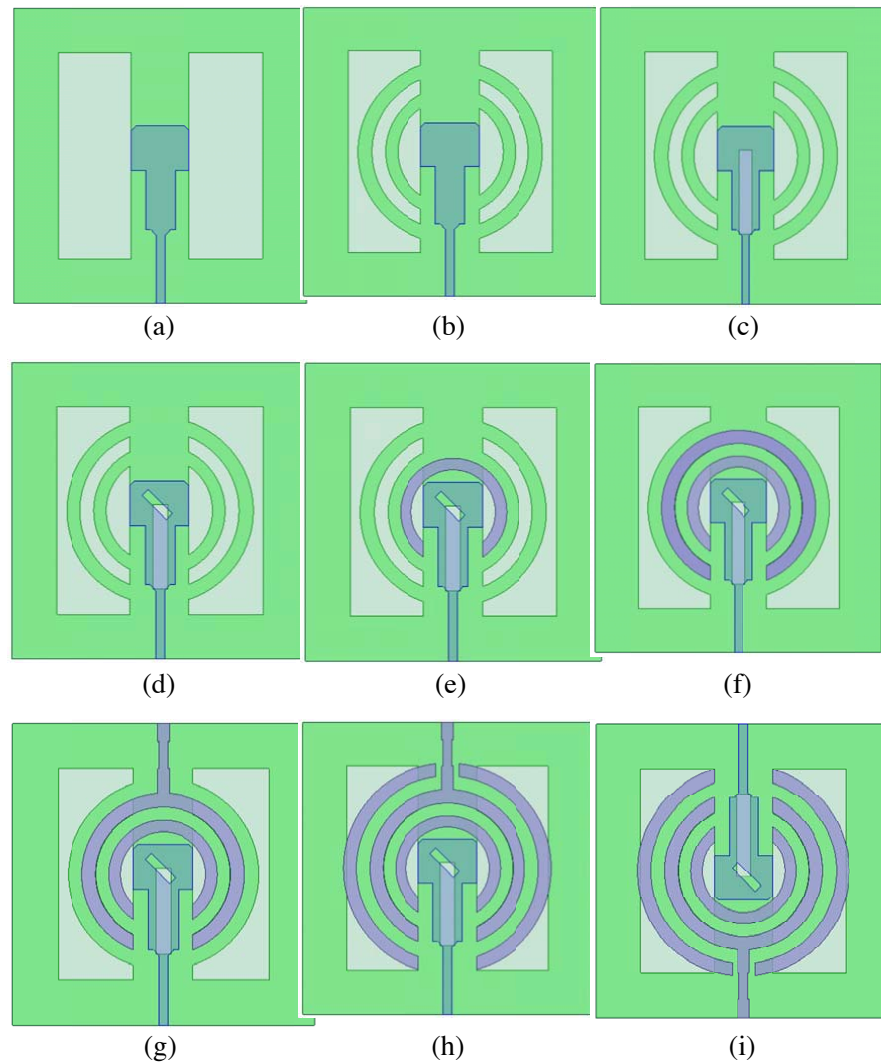
Figure 2. Design stages of the proposed two port antenna.

evolution stage achieves a peak gain of 8.43 dBi in the E-plane. The return loss in dB and E-plane gain of this stage are shown in Figs. 5(a) and 5(b). The next stage (D) is evolved from the 3rd one by adding an oblique slot $(sl \times sw) \, \text{mm}^2$ on the radiating rectangular mini-patch. The return loss in dB and E-plane gain of this stage are shown in Figs. 6(a) and 6(b), respectively. This developmental stage results in a much better return loss of 37.10 dB at 28.06 GHz with an impedance bandwidth of 4.2% and a VSWR value of 1.02. The stage has an RL ≤ 10 dB from 27.43 to 28.61 GHz having a bandwidth of 1.18 GHz. The introduction of the oblique slot results in a much better return loss, good impedance matching, and a higher peak gain of 8.41 dBi than the 2nd stage. The 5th stage (E) is obtained from stage (D) with the introduction of the first microstrip Yagi director around the rectangular mini-patch. The return loss and E-plane gain of this stage are depicted in Figs. 7(a) and 7(b), respectively. With the inclusion of the Yagi director, this developmental stage achieves a return loss value of 35.85 dB at 28.52 GHz with a 10 dB bandwidth of 1.09 GHz from 27.90 to 28.99 GHz. This stage shows a reduction in impedance bandwidth compared to all previous stages to a value of 3.82% but achieves a much higher E-plane peak gain of 10.16 dBi than the previous stages discussed so far. The 6th stage (F) evolves from stage (E) after the inclusion of the 2nd inverse microstrip Yagi director. The respective return loss and E-plane gain of this stage are shown in Figs. 8(a) and 8(b). This stage of the proposed antenna shows two dips in RL vs. frequency curve at 27.14 GHz and 28.76 GHz with return loss values of 12.69 dB
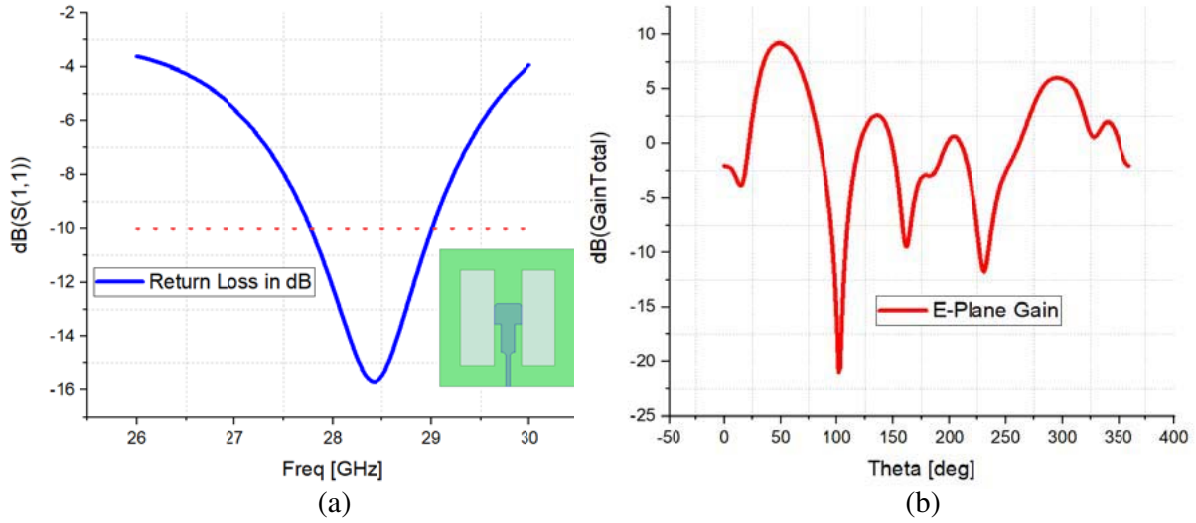
Figure 3. Simulated return loss and E-plane gain of the 1st stage (A).
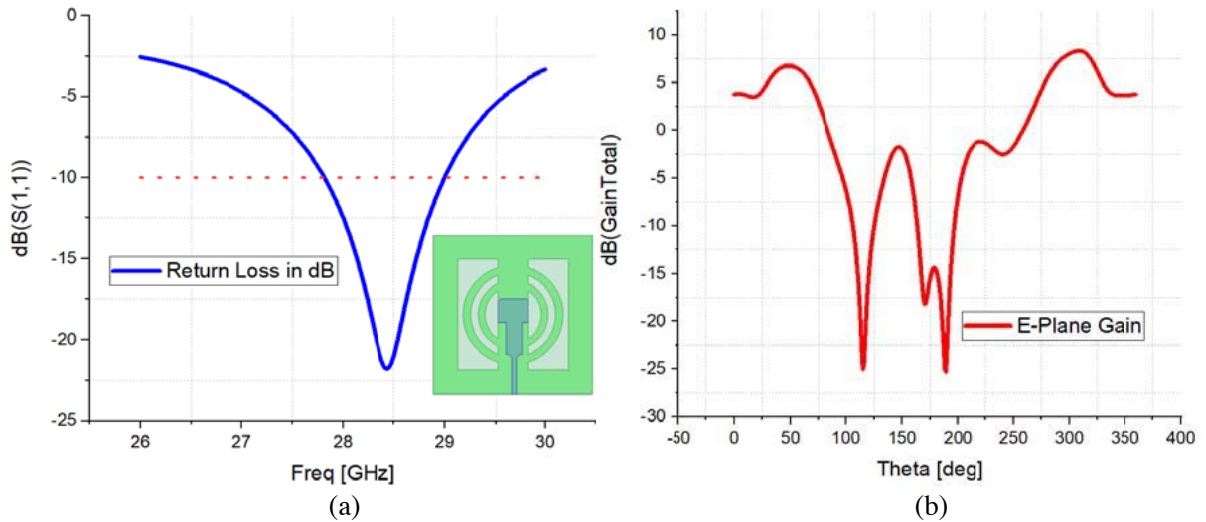
Figure 4. Simulated return loss and E-plane gain of the 2nd stage (B).

and 18.99 dB, respectively. This stage is a matched structure with a VSWR value ranging from 1.2 to 1.6. Besides achieving a high E-plane peak gain of 10.10 dBi, this stage succeeds in achieving a higher impedance bandwidth of 8.62% at a central frequency of 27.24 GHz with RL $\leq$ 10 dB from 26.80 GHz to 29.15 GHz. The 7th stage (G) is obtained from stage (F) by attaching a stepped impedance to the 2nd Yagi director of the 6th stage. With the inclusion of stepped impedance, the stage (G) turns into a two-port antenna. The stepped impedance feeds the 2nd Yagi director from Port 2 and makes the antenna to resonate at 8.42 GHz. This stage of the antenna besides resonating at millimeter-wave frequency of 27.5–28.5 GHz has therefore an added feature to resonate at X-band frequency of 8.42 GHz. The return loss and maximum E-plane gain of this stage when it is employed as a millimeter-wave antenna are depicted in Figs. 9(a) and 9(b) and when it is employed as an X-band antenna shown in Figs. 9(c) and 9(d). From Fig. 9, it can be inferred that the antenna achieves two dips in RL vs. frequency curve at the two resonant frequencies of 26.90 GHz and 28.64 GHz with the return loss values of 12.92 dB and 18.33 dB, respectively. The VSWR value ranges from 1.2 to 1.5, showing a better impedance match in the specified mmWave frequency range. The antenna achieves a peak gain of 9.86 dBi with a much

Figure 5. Simulated return loss and E-plane gain of the 3rd stage (C).
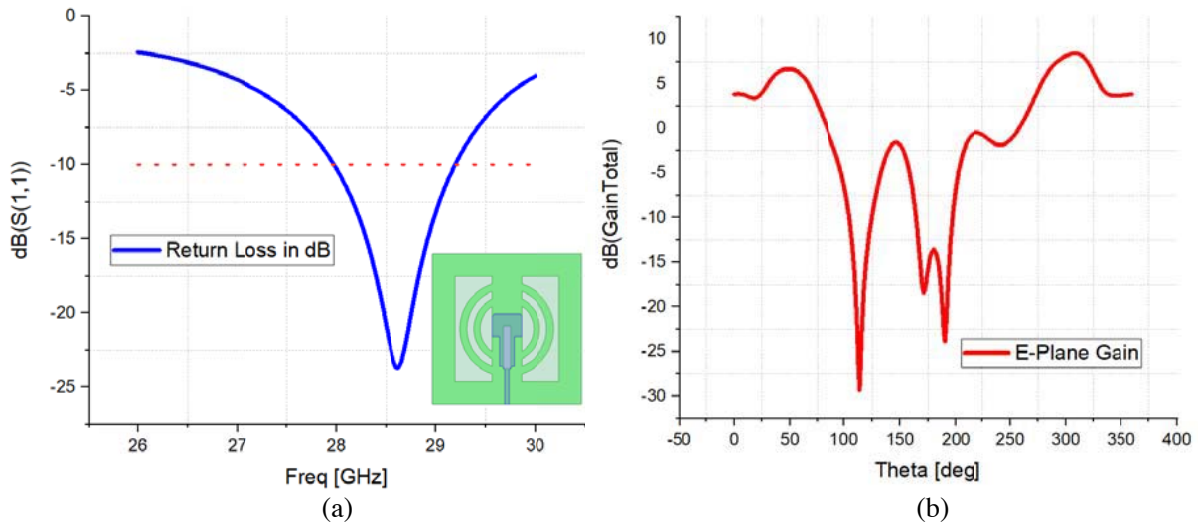
Figure 5. Simulated return loss and E-plane gain of the 3rd stage (C).
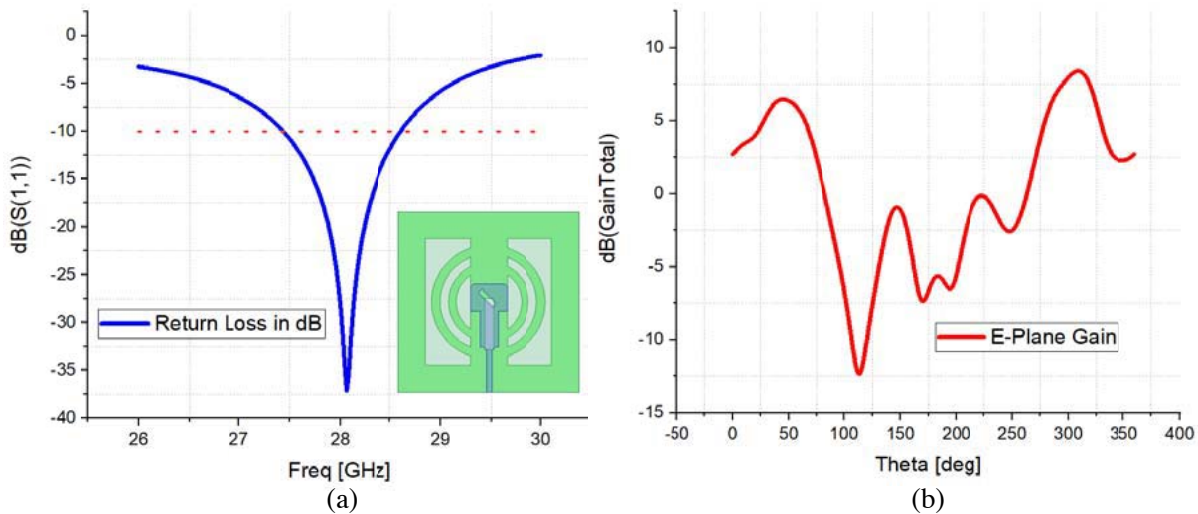
Figure 6. Simulated return loss and E-plane gain of the 4th stage (D).

higher impedance bandwidth of 8.95% at 27.24 GHz than all the previous stages. This stage of the antenna has an RL $\leq$ 10 dB from 26.56 GHz to 29 GHz, achieving a bandwidth of 2.44 GHz. When being employed as an X-band antenna, it resonates at 8.42 GHz with a return loss of 14.04 dB and a VSWR value of 1.49. This stage of the antenna achieves a peak gain of 6.35 dBi at X-band frequency of 8.42 GHz and has RL $\leq$ 10 dB from 8.38 GHz to 8.44 GHz, thereby having a bandwidth of 60 MHz.

The last stage (Proposed) is obtained by adding the 3rd and last microstrip Yagi director to the 7th stage (G). The 3rd director has been split into two symmetrical halves and added on the left and right of stage (G) to make a path for the stepped impedance to be integrated with the 2nd microstrip director. Therefore, the final proposed geometry of the antenna is obtained which is a high gain millimeter-wave antenna resonating at 27.24 GHz and 28.88 GHz with return loss values of 12.34 dB and 17.94 dB, respectively. The proposed antenna forms a matched geometry with a VSWR value of 1.2 to 1.6. From the RL vs. frequency curve shown in Fig. 10(a), it can be seen that the proposed antenna has an RL $\leq$ 10 dB for two resonant bands 26.96–27.57 GHz and 28.24–29.30 GHz, attaining an impedance bandwidth of 2.23% and 3.67% respectively at 27.24 GHz and 28.88 GHz. The proposed

(a)   (b)
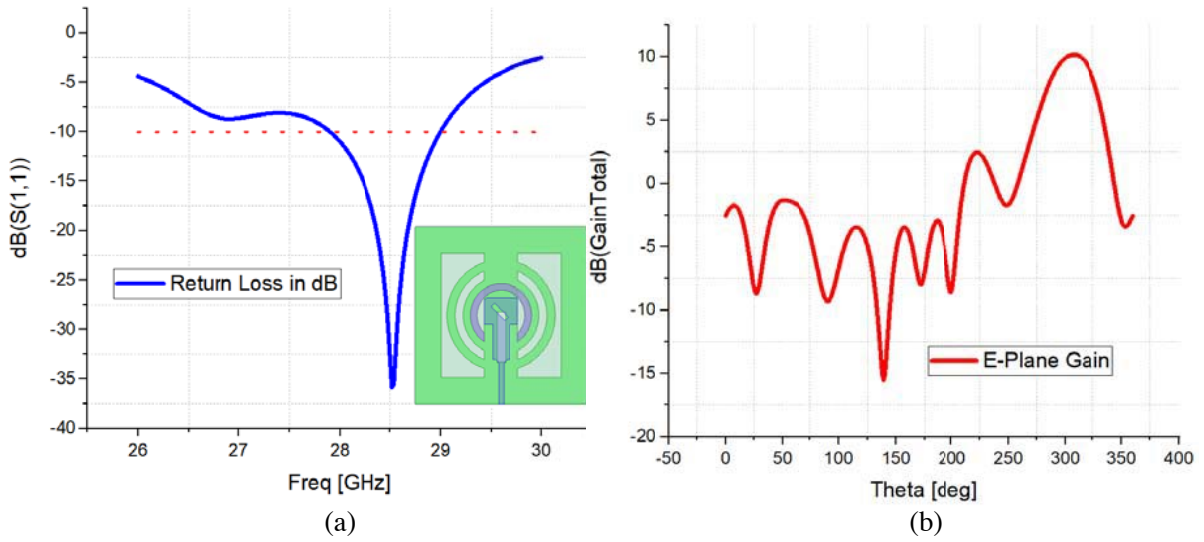
Figure 7. Simulated return loss and E-plane gain of the 5th stage (E).

(a)   (b)
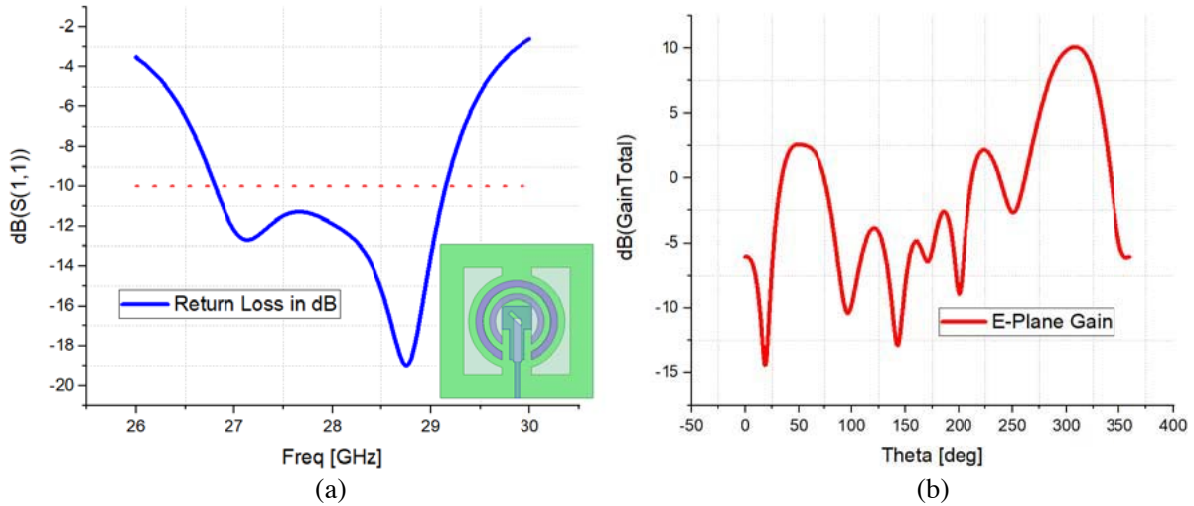
Figure 8. Simulated return loss and E-plane gain of the 6th stage (F).

antenna attains a maximum simulated peak gain of 10.2 dBi in E-plane as depicted from Fig. 10(b). The proposed antenna, when being employed as an X-band antenna, resonates at 8.42 GHz with a simulated return loss of 12.66 dB and a matching VSWR value of 1.6. The antenna attains a maximum E-plane gain of 6.18 dBi. The return loss and E-plane gain of the proposed antenna are depicted in Figs. 10(c) and 10(d). The proposed antenna has a 10 dB return loss value from 8.40 to 8.44 GHz and thus has achieved a bandwidth of 40 MHz in X-band. A comparison of parameters of the proposed antenna and with all the developmental stages from A to G is summarized in Table 2. The data from the table clearly show that the proposed antenna achieves the maximum gain of 10.2 dBi and has a bandwidth of 1.06 GHz, resonating at the two millimeter-wave frequencies of 27.24 GHz and 28.88 GHz with RL $\leq$ 10 dB. Moreover, in Figs. 11(a) and 11(b), the position of the vertical slot on the middle strip of the ground plane is also analyzed to visualize its effect on the return loss and input port impedance of the proposed antenna. From Fig. 11, it can be seen that the antenna attains the best return loss and port impedance value at the slot position of 7.6 mm, but in the finalized geometry the x-coordinate position of the vertical slot has been chosen as 9.6 mm. This position of the slot makes the proposed antenna
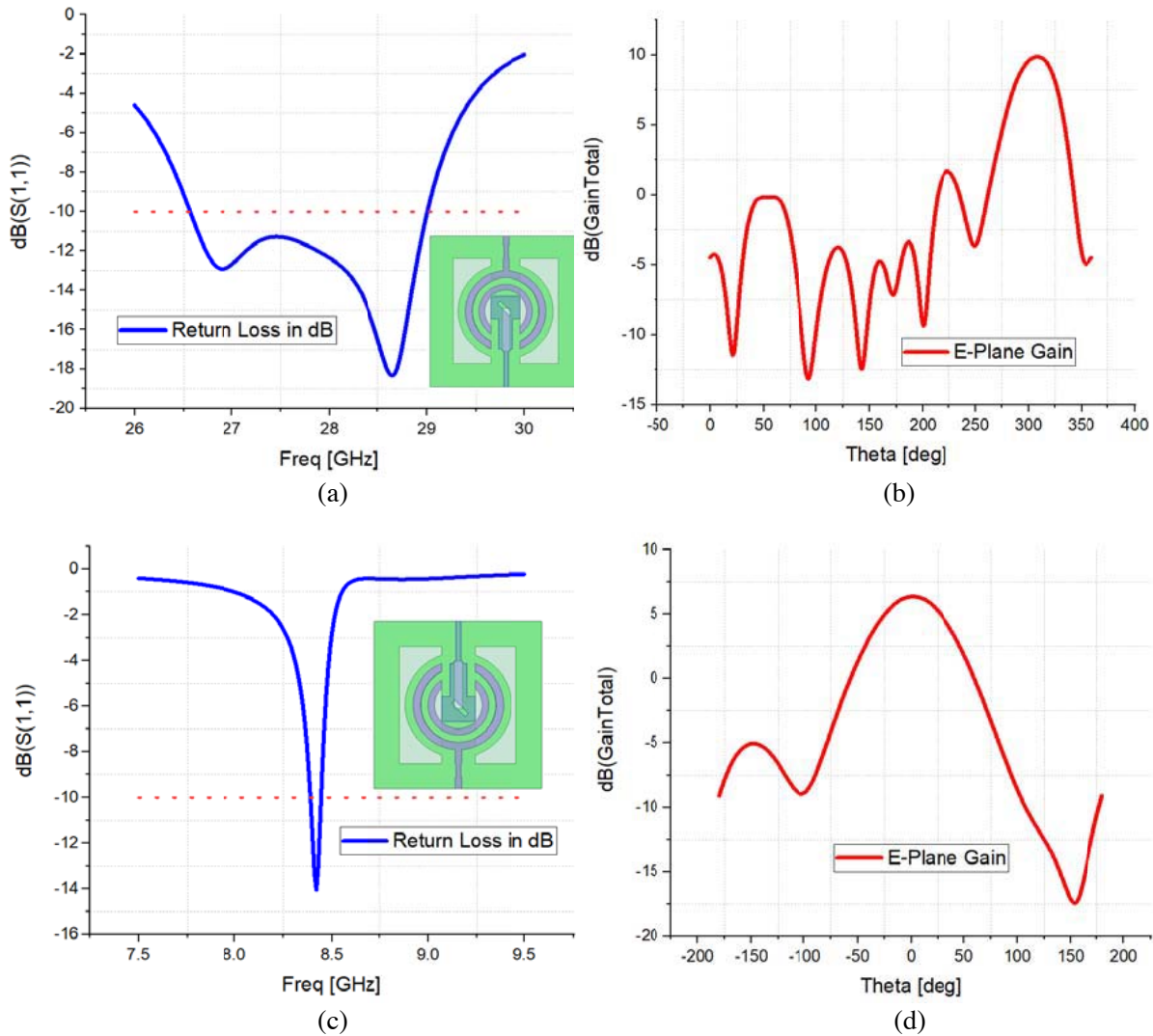
Figure 9. Simulated return loss and E-plane gain of the 7th stage (G). (a), (b) RL and E-plane gain Port 1. (c), (d) RL and E-plane gain Port 2.

achieve the best possible characteristics associated with better gain, better impedance bandwidth, and good radiation efficiency at the two millimeter-wave frequencies of 27.24 GHz and 28.88 GHz. The slot position works equally well for the associated Port 2 impedance of integrated X-band antenna, and hence the proposed two-port antenna achieves a good impedance matching at Port 1 (millimeter-wave port) as well as at Port 2 (Satellite frequency port) leading to a VSWR value of 1.6 at Port 2. Hence, the final proposed profile of the antenna has been devised with the pursual of a keen parametric procedure leading to the development of a novel, low-cost, and compact high gain millimeter-wave antenna with an added feature to be employed as an X-band antenna as well.

In addition, the azimuthal and elevation gains of the proposed antenna for the mmWave band and satellite X-band are shown in Fig. 12. Figs. 12(a) and 12(b) correspond to the excitation at Port 1, and Figs. 12(c) and 12(d) correspond to the excitation at Port 2. From the figure, it is seen that the proposed antenna has almost equal azimuth and elevation gains for the specified mmWave band having the maximum peak gain of 10.20 dBi. For the specified X-band, the azimuth and elevation gains are also equal with the maximum peak gain of 6.16 dBi. From the gain plots of the antenna shown in Fig. 12, the proposed antenna has achieved the maximum azimuth gain at theta = 49° and the maximum elevation gain at phi = 0°, 180° for the specified mmWave band. Similarly, the maximum azimuth gain is achieved
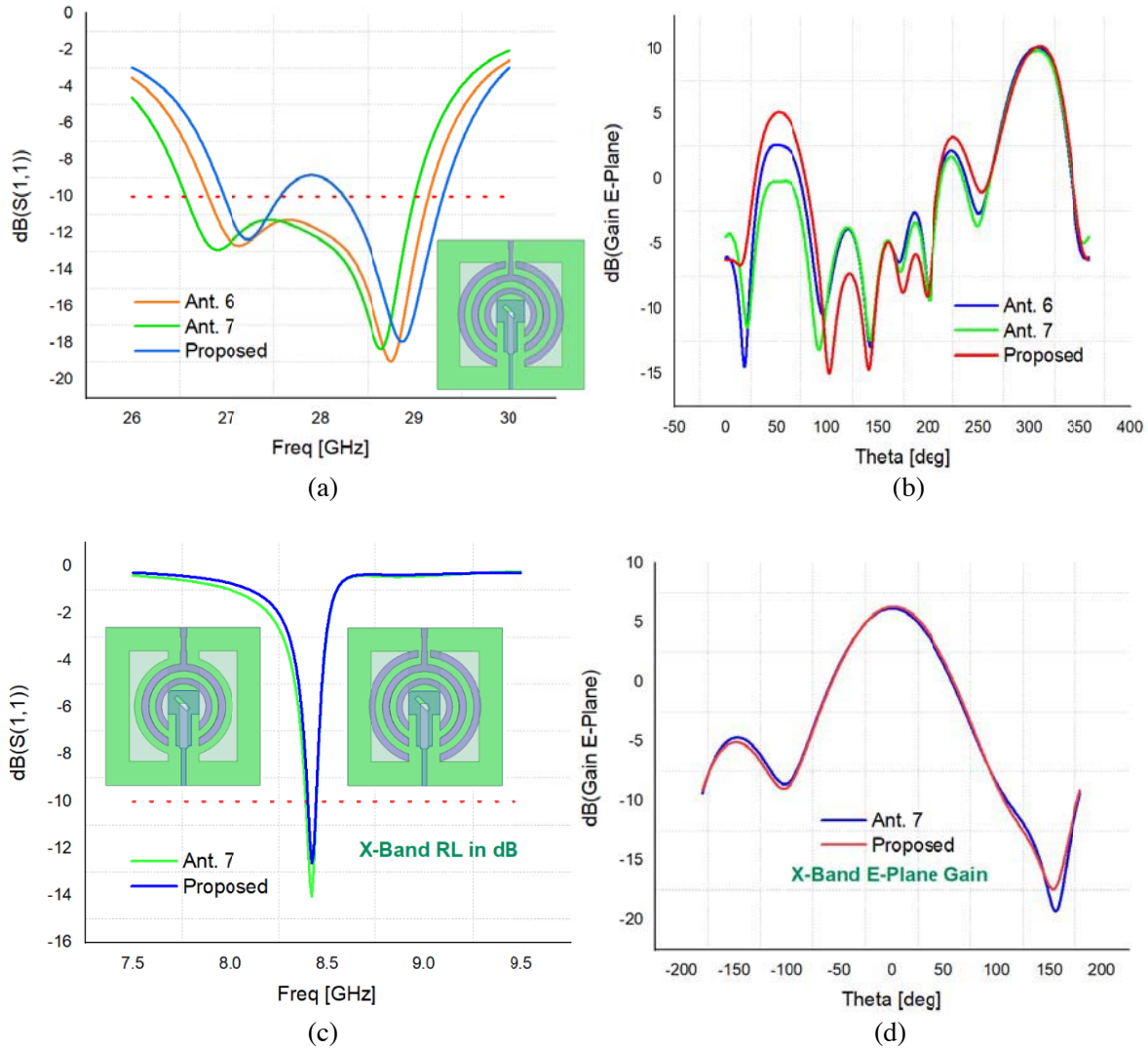
Figure 10. Simulated return loss and E-plane gain of the proposed antenna. (a), (b) RL and E-plane gain with excitation at Port 1. (c), (d) RL and E-plane gain with excitation at Port 2.

at theta $= 0°$, and maximum elevation gain achievement is at phi $= 0°$, $180°$ for the specified X-band. The simulated radiation patterns of the proposed antenna for the specified mmWave bands and the X band frequency are depicted in Figs. 13(a), 13(b) and 13(c), 13(d), respectively. The radiation patterns pertaining to specific phi values $0°$ and $180°$ of the proposed antenna show a good directivity and a high front to back lobe ratio for both the mmWave and X-band frequencies, and for the theta values of $311°$ and $335°$, the proposed antenna achieves two symmetrical beams pointing to $0°$ and $180°$ and a quasi-omni pattern for mmWave band. For the theta values of $5°$ and $25°$, the antenna achieves an omnidirectional pattern and a quasi-omni pattern for the X-band frequency of 8.24 GHz. As can be seen from Figs. 13(a) and 13(b), the proposed antenna when being used as a millimeter-wave antenna has a half-power beam-width (HPBW) of $42°$ for the main radiation beam pointing to $45°$ and an HPBW of $45°$ for the two beams pointing to $0°$ and $180°$, respectively. Similarly, it is observed from Figs. 13(c) and 13(d) that the proposed antenna when being used as an X-band antenna has the HPBW of $62°$ for the main radiation beam pointing towards $0°$ and has an omni-pattern for most of the theta angles like $0°$, $5°$ and quasi-omni pattern for other angles like $25°$.

The Logarithmic surface current distribution of the proposed two-port antenna for its defected

(a)

(b)
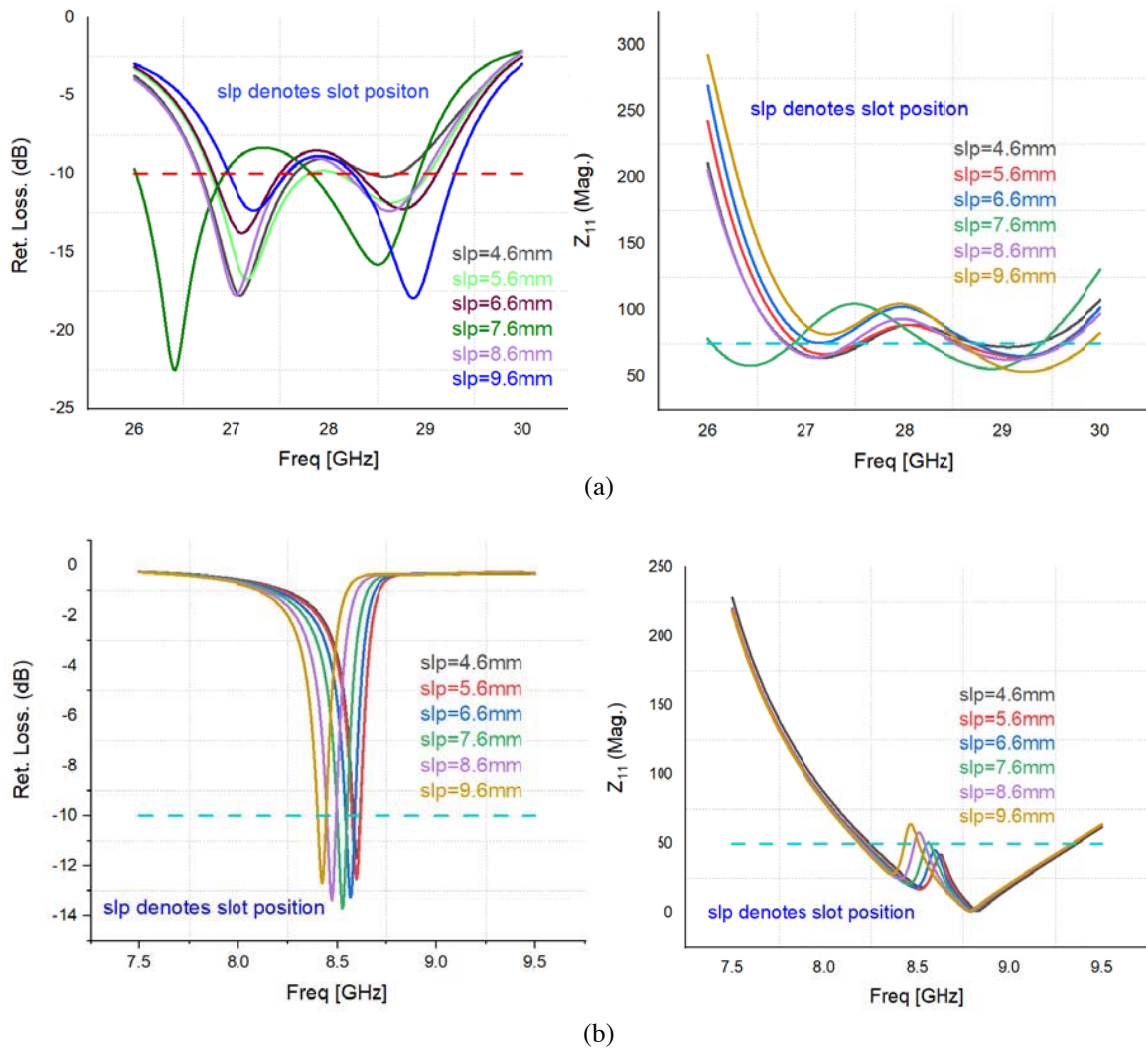
Figure 11. Simulated parametric RL and input impedance of the antenna for varied vertical slot positions.

Table 2. Comparison of parameters of the Finalised proposed antenna with its developmental stages.

Stages of the Proposed Antenna	Resonant Frequency /Band (GHz)	Return Loss in dB	Bandwidth /Impedance Bandwidth	E-Plane Peak Gain (dBi)	Addition of X-band Antenna Section
1st (A)	28.42	15.69	1.23 GHz (4.32%)	9.21	No
2nd (B)	28.44	21.80	1.18 GHz (4.14%)	8.36	No
3rd (C)	28.62	23.72	1.22 GHz (4.26%)	8.43	No
4th (D)	28.06	37.10	1.18 GHz (4.20%)	8.41	No
5th (E)	28.52	35.85	1.09 GHz (3.82%)	10.16	No
6th (F)	26.80–29.15	≤ 10	2.35 GHz (8.62%)	10.10	No
7th (G)	26.56–29	≤ 10	2.44 GHz (8.95%)	9.8	Yes
Proposed	27.24 and 28.88	12.34, 17.94	1.06 GHz (3.67%)	10.20	Yes
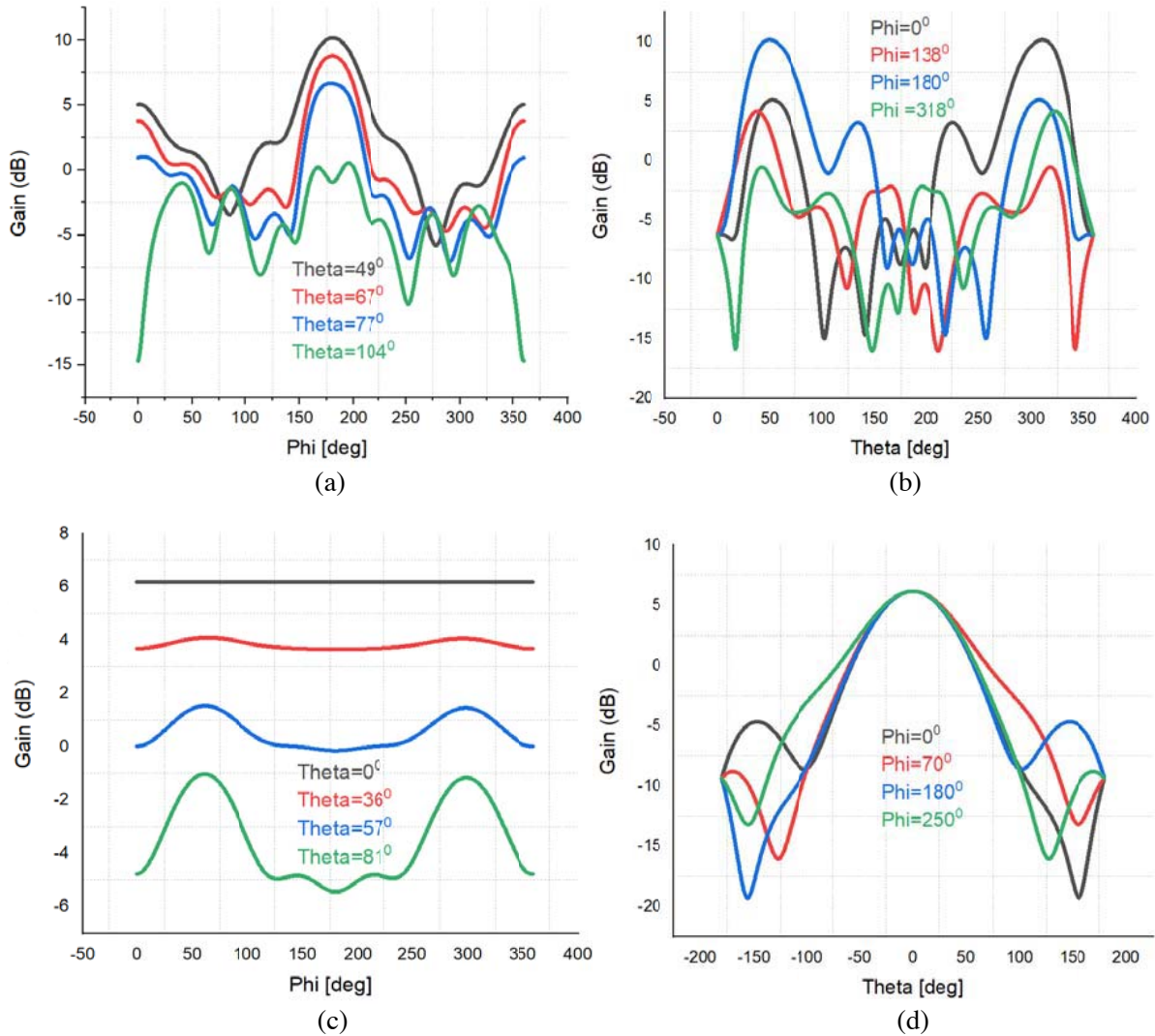
Figure 12. Simulated azimuth and elevation gain of the proposed two-port antenna. (a), (b) Port 1 (mmWave). (c), (d) Port 2 (X-band).

ground and the top radiating mini-patch along with the concentric Yagi directors is shown in Fig. 14. The surface current distribution of the ground plane and top radiating structure at mmWave frequency of 27.24 GHz is depicted in Fig. 14(a), and similarly, Fig. 14(b) depicts the same at X-band frequency of 8.42 GHz. From the figure, it can be seen that the Yagi directors have concentrated the surface current in a specific direction near the mini-patch. The vertical slot on the middle strip of the ground plane elongates the path of the surface current and distributes it towards the upper portions of the strip giving the proposed antenna a good sensing capability to be used as a receiving antenna as well. The unique property of the inverse Yagi directors employed in the proposed design concentrates the EM waves in a specific direction. This makes the proposed antenna achieve much higher gain, high front-to-back lobe ratio, and better directivity providing a strong reason for it to be employed in the millimeter-wave band usually demanding the Line-of-sight communication between the sender and receiver.

4. FABRICATION AND MEASUREMENTS

The final proposed millimeter-wave antenna with added X-band antenna section is fabricated on a 0.8 mm thick Rogers 5880 substrate and is fitted with an SMA connector whose photographs are shown
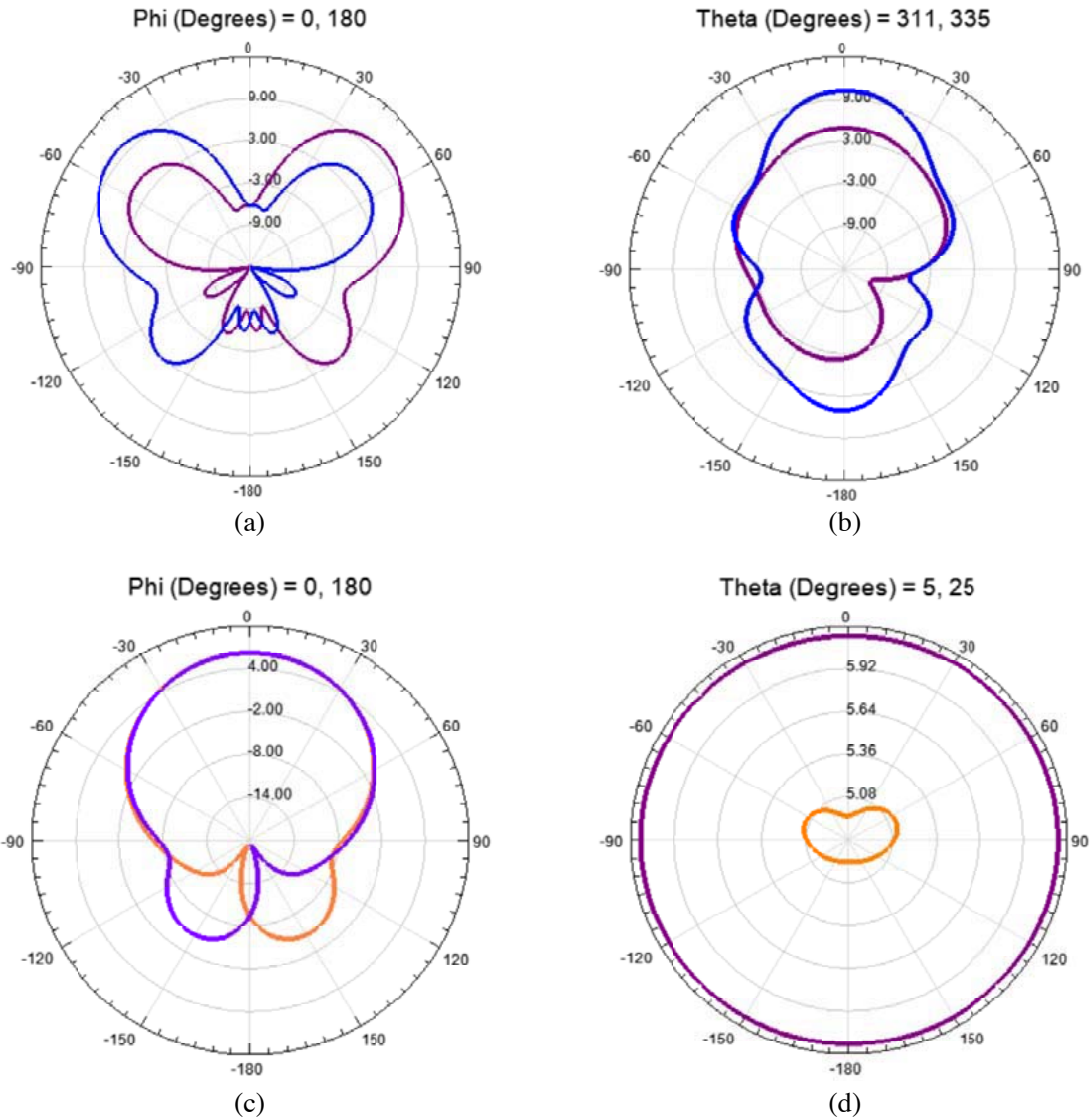
Figure 13. Radiation patterns of the presented two-port antenna. (a), (b) 27.24 GHz, (c), (d) 8.42 GHz.

in Figs. 15(a) and 15(b). The simulated and measured return Losses (RLs) in dB of the antenna are shown in Figs. 15(c) and 15(d) corresponding to specified mmWave band and X-band, respectively. From the return loss vs. frequency curve, it has been observed that the simulated and measured RLs of the proposed antenna for Port 1 (mmWave Port) and Port 2 (X-band Port) are in good agreement. From the comparison of measured and simulated RL values from Figs. 15(c) and 15(d) of the proposed antenna, the measured RL values shown for mmWave Port 1 and X-band Port 2 show a little deviation in the resonant frequencies from the simulated ones. This deviation occurs due to the soldering between SMA connectors and the fabricated antenna. The proposed antenna attains measured RL values of 14.56 dB and 16.06 dB for the resonant frequencies of 27.18 GHz and 28.76 GHz respectively for Port 1 and a measured RL value of 13.34 dB for the resonant frequency of 8.47 GHz for Port 2. The simulated RL values of 12.34 dB and 17.94 dB for the resonant frequencies of 27.24 GHz and 28.88 GHz respectively for Port 1 and a simulated RL value of 12.66 dB for the resonant frequency of 8.42 GHz for Port 2 are depicted from Figs. 15(c) and 15(d), respectively. The maximum measured impedance bandwidth of 3.05% to 3.79% has been obtained whereas the simulated bandwidth is 2.23% to 3.67% for the specified mmWave band of 26.84–29.18 GHz. Similarly, for the specified X-band frequency the measured bandwidth is 50 MHz whereas the simulated bandwidth is 40 MHz only. Figs. 16(a) and 16(b) show

(a)

(b)
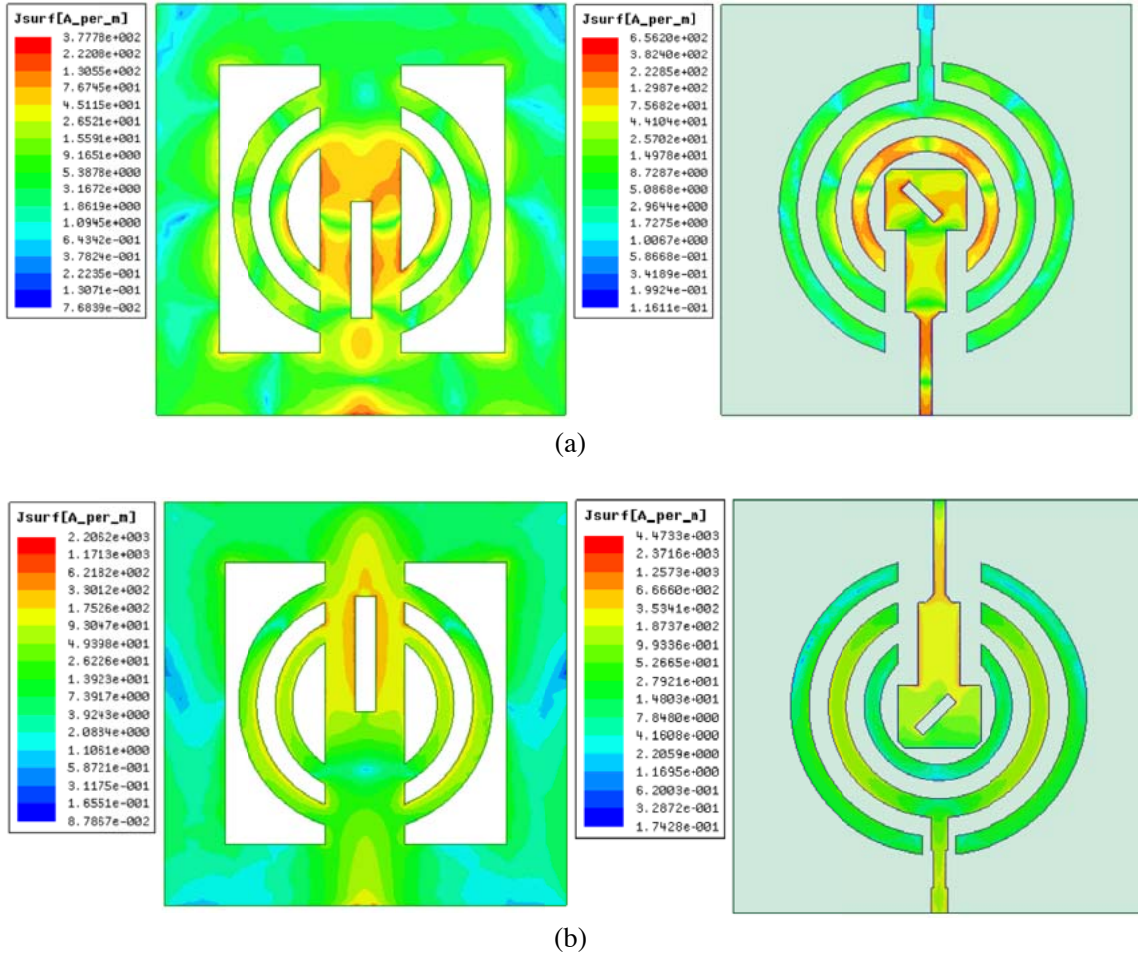
Figure 14. Surface current distribution of the proposed two-port antenna. (a) 27.24 GHz, (b) 8.42 GHz.

the simulated and measured radiation patterns of the proposed antenna for specified mmWave band frequency and X-band frequency with a good matching between the simulated and measured values. The E-plane (XZ-plane) radiation patterns of the proposed antenna for both the mmWave and X-band satellite frequencies have a good directivity as can be seen from Figs. 16(a) and 16(b) whereas a better directivity for the H-plane (YZ-plane) has been obtained for the X-band satellite frequency only. The proposed antenna has obtained a high gain of 10.2 dBi in E-plane only for the mmWave frequency of 27.24 GHz whereas, for the X-band satellite frequency of 8.42 GHz, the antenna obtains a maximum gain of almost 6.2 dBi for both the XZ and YZ planes. The main beam in the E-plane (XZ-plane) is pointed towards 45° and has a half-power beam-width (HPBW) of 42 degrees showing a good directivity at specified mmWave frequency of 27.24 GHz. For H-plane (YZ-plane), at 27.24 GHz, the antenna does not have very much directivity in a particular direction but shows two beams in simulated pattern pointing towards $-155°$ and $+155°$ and in measured pattern has a main beam pointing towards 90 degrees with a scan angle of $+20°$ to $+16°$. The XZ (E-plane) and YZ (H-plane) planes of the proposed antenna at X-band frequency of 8.42 GHz show almost similar radiation patterns with an HPBW of almost 63 degrees.

The simulated and measured gains of the proposed antenna for the specified mmWave band and X-band are depicted in Figs. 17(a) and 17(b), and the simulated radiation efficiency and directivity for these bands are shown in Figs. 17(c) and 17(d). From the relevant figures of Fig. 17, it can be seen that the measured and simulated gains of the proposed two-port antenna are almost the same at the central frequency of 27.24 GHz of mmWave band and at central frequency of 8.42 GHz of satellite X-band. At higher frequencies greater than 27.24 GHz and 8.42 GHz, the measured gain shows a decrement of
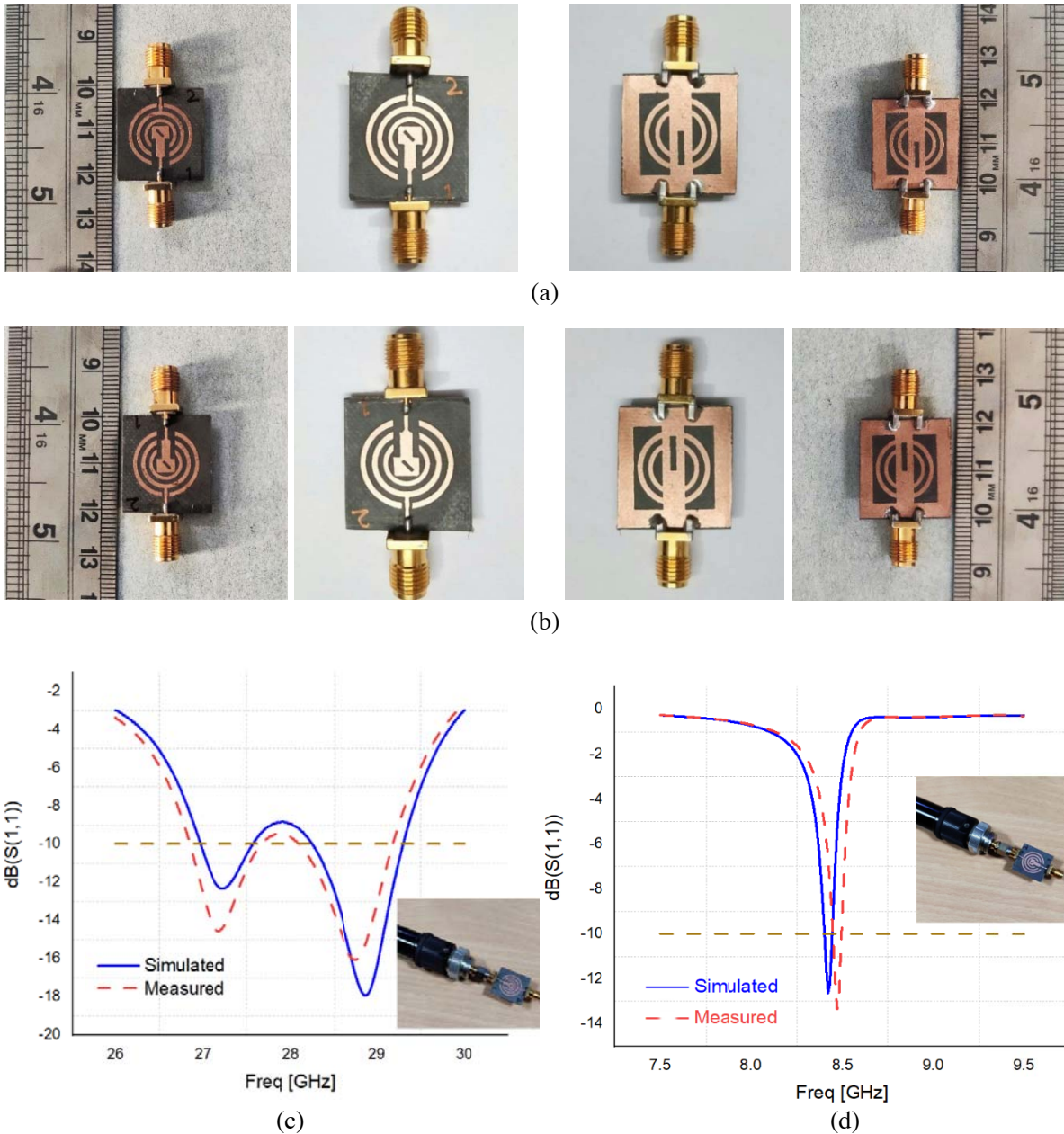
Figure 15. Fabricated proposed antenna with simulated and measured values.

the order of 0.1–0.2 dBi, and hence the proposed antenna achieves the peak gain values of 10.2 dBi and 6.2 dBi, respectively. Moreover, the simulated 3D radiation patterns of the proposed antenna for mmWave frequency of 27.24 GHz and the satellite X-band frequency of 8.42 GHz are depicted in Fig. 18. The 3D pattern has been obtained by the combined sweep of both the azimuth and elevation angles from 0–360 degrees. As can be seen from the figure, the main radiation lobe at mmWave frequency is at an angle of about 30 degrees with the positive direction of Z-axis, and for the X-band frequency, it is along Z-axis perpendicular to the plane containing the antenna. The simulated radiation efficiency of the proposed antenna in mmWave band depicted in Fig. 17(c) ranges from 98 to 99% with the peak directivity value of 10.26 dB while in the X-band specified depicted in Fig. 17(d), it varies from 68 to 98% with the peak directivity value of 6.02 dB. The gain of the proposed antenna varies from 5.8 to 10.2 dBi and 3.8 to 6.2 dBi in respective mmWave and satellite frequency bands with higher radiation

(a)

Simulated
Measured

(b)
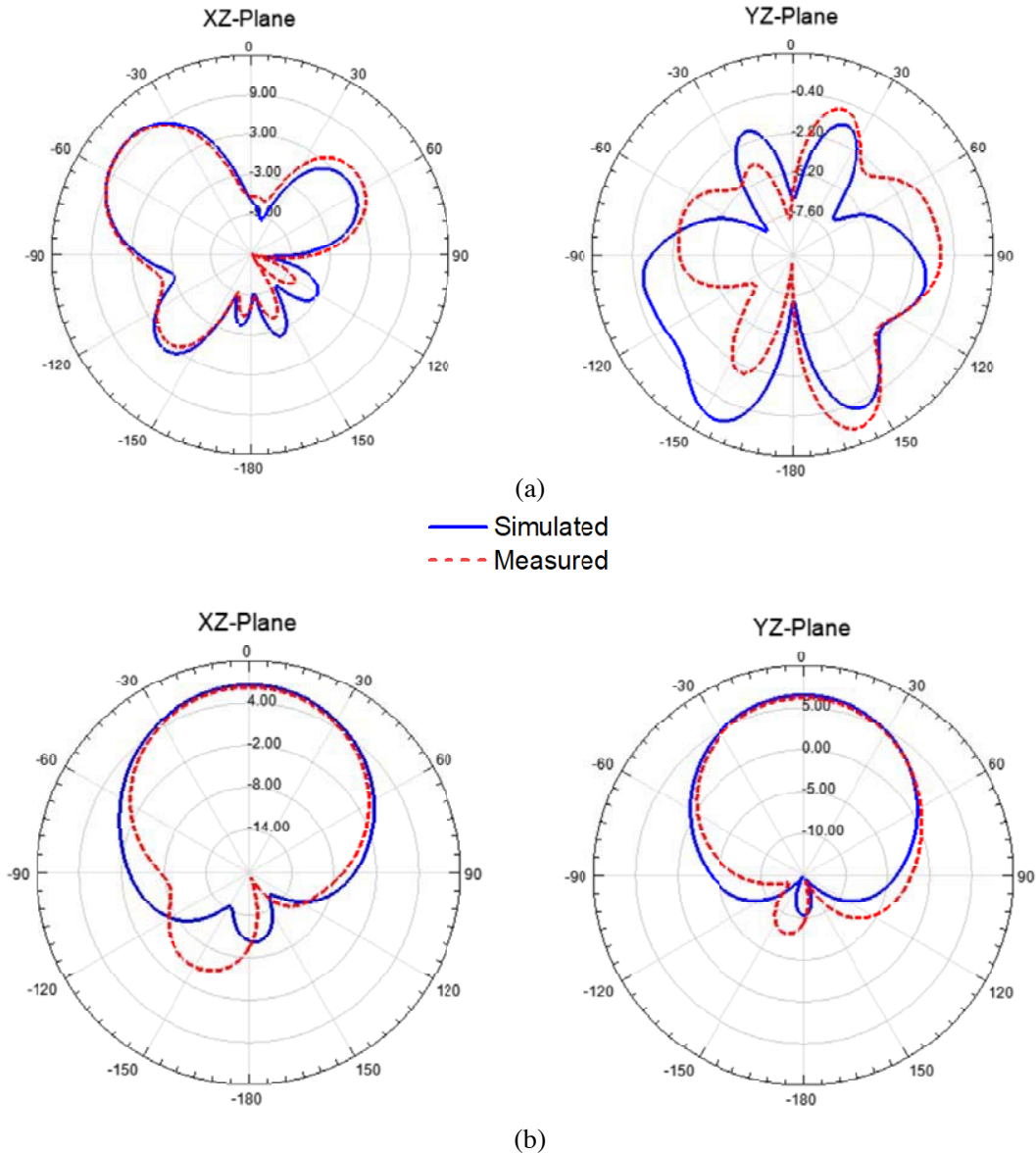
Figure 16. Simulated and measured radiation patterns of the presented two-port antenna. (a) 27.24 GHz, (b) 8.42 GHz.

efficiency. In addition, the antenna has obtained a high isolation of 15–25 dB between the two ports as can be observed from Fig. 19 giving it an added advantage to operate simultaneously for both frequencies of mmWave and satellite X-band. Photographs of the proposed antenna inside an anechoic chamber during measurement are shown in Fig. 20.

5. STATE OF ART COMPARISON

To validate the effectiveness and validity of the work, the proposed antenna is compared with the previous reported antennas, and the comparison is depicted in Table 3. The proposed antenna has far better characteristics regarding peak gain, simple planar geometry, impedance bandwidth, operating frequency, and most importantly its utilization in the millimeter-wave band of 26.5–28.5 GHz because of its compact, novel, and highly miniaturized structure suitable for integration with other millimeter-wave frequency circuits.
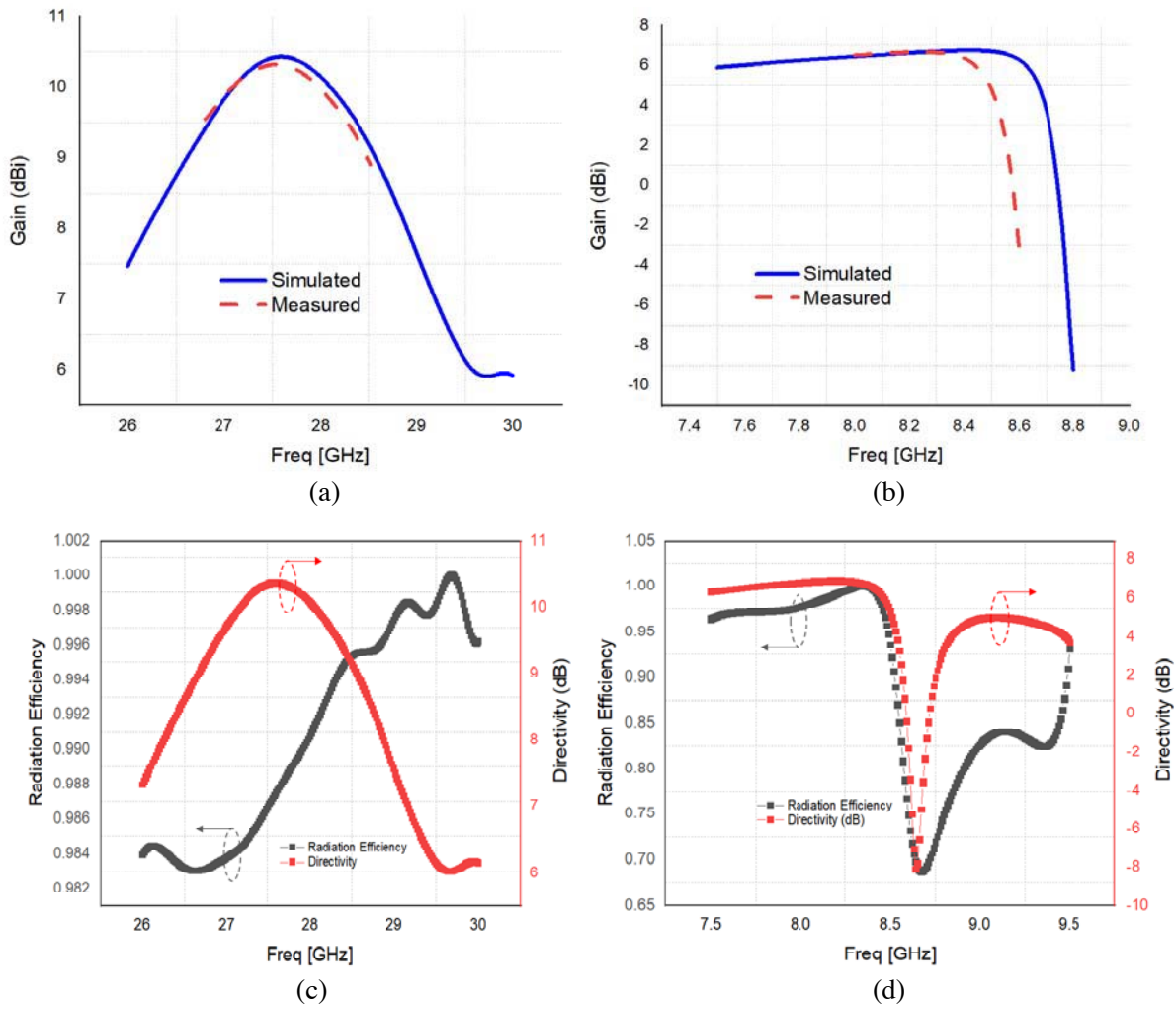
Figure 17. Gain of the proposed two-port antenna with simulated radiation efficiency and directivity.

27.24 GHz

8.42 GHz
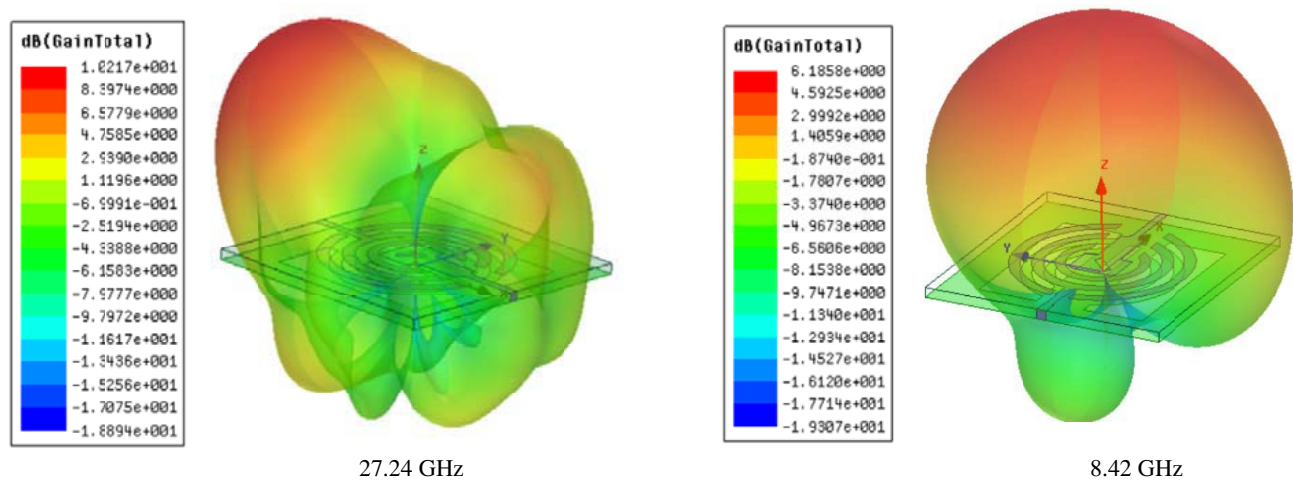
Figure 18. 3D radiation patterns of the proposed antenna at mmWave and X-band frequency.
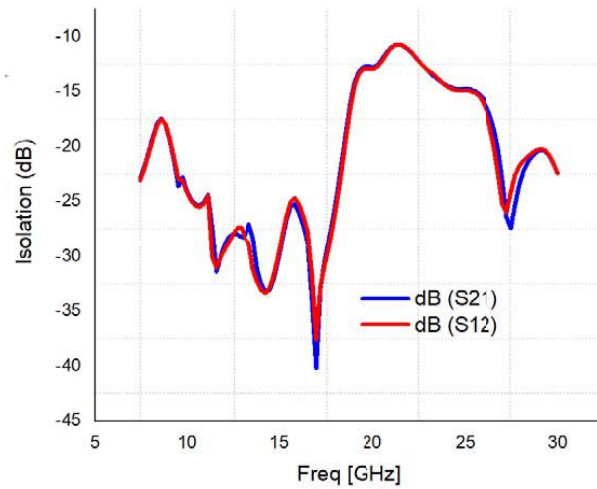
Figure 19. Isolation between two ports of the presented antenna.
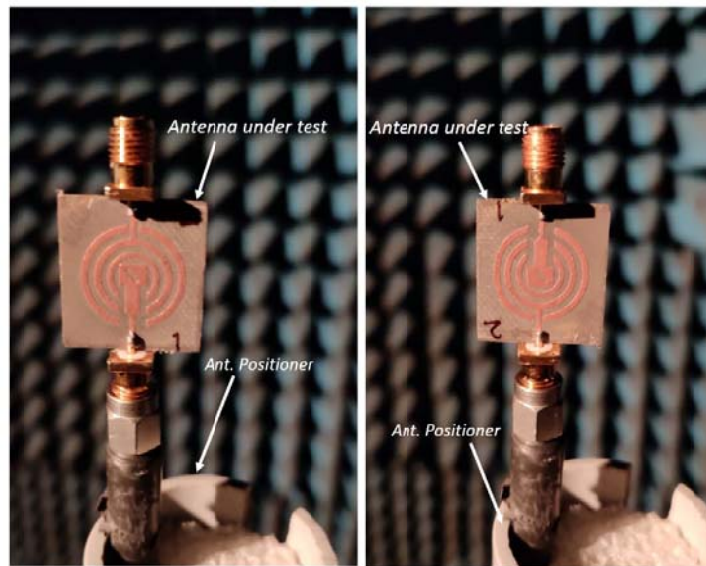
Figure 20. Photograph of the proposed two-port antenna under test inside an anechoic chamber.

Table 3. Proposed antenna compared with previous reported antennas.

Ref./Year	Freq. band (GHz)	Impedance bandwidth	Peak gain (dBi)	Type
[11]/2018	39–49.3	22.9%	5.5	SIW/Reflector Omni
[13]/2017	24–32	47%	9	SIW/Tapered Slot
[15]/2016	57–67	-	2.2	Loop Micro-strip
[12]/2021	25–29/36–41	13%	5/5.7	Planar/Monopole
Proposed work	26.96–29.30/8.2–8.4	3.79%	10.2/6.2	Planar/low-cost Concentric Yagi Circular

6. CONCLUSION

A novel and high gain compact antenna employing a concentric inverse Yagi geometry has been designed and fabricated successfully over a Rogers RT 5880 substrate having a miniaturized dimension of $20 \times 20 \, \text{mm}^2$. The simulated results of the antenna are compared with the measured ones and found in good agreement. The antenna succeeds in achieving a high gain of $10.2 \, \text{dBi}$ for mmWave band and a gain of $6.2 \, \text{dBi}$ for satellite X-band. The achievement of impedance bandwidth is 3.79% for the specified mmWave band. The peak gain of the antenna achieves the highest value for E-plane with better directivity. Moreover, almost equal E-plane and H-plane gains for the satellite X-band are found providing polarisation diversity to be used for WGS satellite system. The Yagi geometry makes the antenna achieve an appreciable high gain requirement of the millimeter-wave band with better impedance matching and makes it achieve the added feature to resonate in the satellite X-band as well. The antenna is proved to be very efficient in terms of radiation efficiency, good isolation between the two ports, cost reduction, high miniaturization with good sensing capability for incoming radiation making the proposed antenna serve as a sterling candidate for 5G millimeter-wave communication and also for WGS satellite system providing the capacity for both X and Ka bands simultaneously for military applications.

REFERENCES

1. Ayanoglu, E., A. L. Swindlehurst, P. Heydari, and F. Capolino, "Millimeter-wave massive MIMO: The next wireless revolution," *IEEE Communications Mag.*, Vol. 52, No. 9, 56–62, 2014.
2. Rappaport, T. S., R. H. Mayzus, and S. Zhao, "Millimeter-wave mobile communications for 5G: It will work!," *IEEE Acces.*, Vol. 1, No. 1, 225–349, 2013.
3. Roh, W., J. Park, J. H. Park, and J. Y. Seol, "Millimeter-wave beam-forming as an enabling tech. for 5G cellular communications: Theoretical feasibility & prototype results," *IEEE Com.*, Vol. 52, No. 2, 106–113, 2016.
4. Kim, Y. and H. Lee, "Feasibility of mobile cellular communications at millimetre wave frequency," *IEEE Journ. of Selected Topics in Signal Procesg.*, Vol. 10, No. 3, 589–599, 2016.
5. Wang, H., D. G. Fang, B. Zhang, and W. Q. Che, "Dielectric loaded SIW H-plane horn antennas," *IEEE Trans. Antennas and Propa.*, Vol. 58, No. 3, 640–647, 2010.
6. Li, M. and K. M. Luk, "Wideband 60-GHz magneto-electric dipole antenna for mmWave communications," *IEEE Trans. Antennas and Propa.*, Vol. 63, No. 7, 3276–3279, 2015.
7. Zhang, Y., X. Qing, Z. N. Chen, and W. Hong, "Wideband mmWave SIW slotted narrow-wall fed cavity antennas," *IEEE Trans. Antennas and Propa.*, Vol. 59, No. 5, 1488–1496, 2011.
8. Yang, T. Y., W. Hong, and Y. Zhang, "Wideband mmWave SIW cavity-backed rectangular patch antenna," *IEEE Anten. Wireless Propag. Lett.*, Vol. 13, No. 13, 205–208, 2014.
9. Djerafi, T. and K. Wu, "Corrugated substrate integrated waveguide (SIW) antipodal linearly tapered slot antenna array fed by quasi-triangular power divider," *Progress In Electromagnetics Research C*, Vol. 26, 139–151, 2012.
10. Ghiotto, A., F. Parment, K. Wu, and T. P. Vuong, "Millimeter-wave air-filled substrate integrated waveguide antipodal linearly tapered slot antenna," *IEEE Anten. Wireless Propag. Lett.*, Vol. 24, No. 5, 1–4, 2016.
11. Fan, K., Z.-C. Hao, Q. Yuan, J. Hu, G. Q. Luo, and W. Hong, "Wideband horizontally polarized omni-directional antenna with a conical beam for millimeter-wave applications," *IEEE Trans. Antennas and Propa.*, Vol. 66, No. 9, 4437–4448, 2018.

12. Ali, W., S. Das, H. Medkour, and S. Lakrit, "Planar dual-band 27/39 GHz millimeter-wave MIMO antenna for 5G applications," *Microsystem Tech.*, Vol. 27, No. 1, 283–292, 2021.

13. Yang, B., et al., "Compact tapered slot millimeter-wave antenna array for massive MIMO 5G systems," *IEEE Trans. Antennas and Propa.*, Vol. 65, No. 12, 6721–6727, 2017.

14. Kumar, A., M. S. Mahendra, and P. Y. Rajendra, "Dual wideband circular polarised CPW-fed strip and slots loaded compact square slot antenna for wireless and satellite applications," *AEU-International Journ. of Electronics and Commun.*, Vol. 108, 181–188, 2019.

15. Ghazizadeh, M. H. and M. Fakharzadeh, "60 GHz omni-directional segmented loop antenna," *IEEE Internat. Symp. on Ant. and Propagation*, 1653–1654, Fajardo, U.S.A, June–July 2016.

16. Rehman, R., J. A. Sheikh, and Z. A. Bhat, "A novel high gain two port antenna for licensed and unlicensed millimeter-wave communication," *2020 IEEE International Conference on Emerging Trends in Information Technology and Engineering (ic-ETITE)*, 1–5, Vellore, India, February 2020.

17. Zhou, Z., Z. Wei, Z. Tang, and Y. Yin, "Design and analysis of a high isolation wideband multiple-microstrip antenna dipole," *IEEE Anten. Wireless Propag. Lett.*, Vol. 18, No. 4, 722–726, 2019.

18. Tang, M. C., et al., "Compact tri-polarization diversity wideband, reconfigurable and wideband filtenna," *IEEE Trans. Antennas and Propa.*, Vol. 67, No. 8, 5689–5694, 2019.

19. Wang, J., et al., "Graphene-based microwave antennas with reconfigurable pattern," *IEEE Trans. Antennas and Propa.*, Vol. 68, No. 4, 2504–2510, 2019.

20. Hussain, S., S. W. Qu, W. L. Zhou, P. Zhang, and S. Yang, "Design and fabrication of wideband dual-polarized dipole array for 5G wireless systems," *IEEE Acces.*, Vol. 8, 65155–65163, 2020.

21. Wu, G. B., et al., "High-gain filtering reflect-array antenna for millimeter-wave applications," *IEEE Trans. Antennas and Propa.*, Vol. 68, No. 2, 805–812, 2020.

22. Farahat, A. E. and K. F. A. Hussein, "28/38 GHz dual-band Yagi-Uda antenna with corrugated radiator and enhanced reflectors for 5G MIMO antenna systems," *Progress In Electromagnetics Research C*, Vol. 101, 159–172, 2020.

23. Kaur, A. and P. K. Malik, "Multiband elliptical patch fractal and defected ground structures microstrip patch antenna for wireless applications," *Progress In Electromagnetics Research B*, Vol. 91, 157–173, 2021.